Takedown
If you consider content in White Rose Research Online to be in breach of UK law, please notify us by emailing eprints@whiterose.ac.uk including the URL of the record and the reason for the withdrawal request.

eprints@whiterose.ac.uk
https://eprints.whiterose.ac.uk/

1 **Understanding dust sources through remote sensing: making a case for**

2 **CubeSats**

3

4 Matthew C. Baddock[1*], Robert G. Bryant[2], Miguel Domínguez Acosta[3] and Thomas E. Gill[4]

5

6 [1]Geography and Environment, Loughborough University, Loughborough, LE11 3TU, UK

7 [2]Geography, University of Sheffield, Sheffield, S10 2TN, UK

8 [3]Ingenieria Civil y Ambiental, Universidad Autonoma de Ciudad Juarez, 450 N. Avenida del

9 Charro, Ciudad Juarez, Chihuahua, 32315, Mexico

10 [4]Geological Sciences, University of Texas at El Paso, 500 W. University Avenue, El Paso,

11 TX, 79968, USA

12 *Email: m.c.baddock@lboro.ac.uk

13

14 ABSTRACT

15 Dust sources have been revealed through remote sensing, first regionally by ~1°

16 resolution sensors (TOMS), then at sub-basin scale by moderate-resolution sensors

17 (MODIS). Sensors with higher spatial resolution until recently were poorly

18 temporally-resolved, precluding their use for systematic investigations of sources.

19 Now, "CubeSat" constellations with high-temporal-and-spatial-resolution sensors

20 such as PlanetScope offer ~3 m resolution and daily (to sub-daily) temporal

21 resolution. We illustrate the spatio-temporal dust plume observation capabilities of

22 CubeSat data through a dust event case study, Bolson de los Muertos playa,

23 Chihuahuan Desert, Mexico. For the event, PlanetScope showed numerous discrete

24 point sources, revealing variability of surface erodibility and emission over ~8% of a

25 focus area at time of capture. The unprecedented detail of PlanetScope imagery

26 revealed plume development where outer-playa sands and fluvial-deltaic inputs

27 contact lacustrine silts/clays, consistent with field-studies. PlanetScope's high fidelity

28 improves spatial quantification and temporal constraint of source activity, and we
29 assess the spatio-temporal capabilities of CubeSat in context with other dust
30 observation remote sensing systems. Compared to previous satellite technologies,
31 CubeSats bring better potential to link remote sensing to field observations of
32 emission. This leap forward in the remote sensing of dust sources calls for the
33 systematic analysis of CubeSat imagery in source areas.

34

35 Keywords: mineral aerosol, PlanetScope, MODIS, Chihuahuan Desert, dust
36 emission, playa

37

38 1. INTRODUCTION

39 For a more comprehensive understanding of the mineral dust cycle, there is a
40 recognised need for improved spatio-temporal constraint on the sources of dust
41 emission and their dynamics (Zender *et al.*, 2003; Bullard *et al.*, 2011; Shao *et al.*,
42 2011; Heinold *et al.*, 2016). Many of the fundamental properties of dust that govern
43 its potential environmental impacts (i.e., particle size, mineral and chemical
44 composition) are influenced by the particular source area it is emitted from. Sources
45 are thus the 'launch pads' of mineral dust, and represent the start of its atmospheric
46 lifecycle. Field-based observation of dust emission at source, however, is not
47 straightforward, given the often remote and harsh environments where sources
48 occur, as well as the dynamic and complex spatio-temporal nature of emission
49 processes (Thomas and Wiggs, 2008; Field *et al.*, 2009; Bullard, 2010; Bryant,
50 2013).

51

52 *1.1. Remote sensing of dust sources: a brief review*

53 Remote sensing has long provided significant advances in understanding the spatial
54 distribution and temporal variability exhibited by contemporary dust sources.
55 Improvements in spatial fidelity of sensors have in particular provided an impetus for
56 interpreting the dust cycle and the nature of dust sources. The first multi-annual,
57 global remote sensing studies of atmospheric dust loading established the dominant

58 large-scale source regions, revealing the importance of closed hydrological basins

59 (Prospero *et al.*, 2002; Washington *et al.*, 2003). Such basins were either inundated

60 during the Pleistocene and/or undergo ephemeral flooding in modern climates,

61 storing accumulated fines, the deflation of which makes them major sources (high

62 frequency and/or high magnitude emission) of mineral dust. The Total Ozone

63 Mapping Spectrometer (TOMS) provided landmark characterisation of dust sources

64 in the early 2000s at a spatial resolution of ~1° ° (Prospero *et al.*, 2002; Washington

65 *et al.*, 2003). Subsequent time-series observations of dust at this scale revealed the

66 intermittency and interannual variability of emission from key source regions,

67 especially those outside of the principal Saharan Dust Belt (Mahowald *et al.*, 2003;

68 Zender *et al.*, 2003; Bryant *et al.*, 2007; Mahowald *et al.*, 2010). Following the

69 identification of major dust-emitting basins, ensuing remote sensing investigations of

70 source regions focused on finer spatial scales, notably adopting a sub-basin scale of

71 enquiry. This "drilling down" was motivated by knowledge that while individual, often

72 huge, basins were identifiable as single large-scale entities, the actual locations of

73 dust emission occurred at much smaller spatial scales within them, preferentially

74 linked to certain geomorphology and surface types (Bullard *et al.*, 2008; 2011).

75

76 Sub-basin focused studies were driven by improvements in sensor technology,

77 especially the early-2000s advent of the daily (later twice daily) 0.25-1 km resolution

78 hyperspectral Moderate Resolution Imaging Spectroradiometer (MODIS) (Muhs *et*

79 *al.*, 2014). The spatial scale offered by MODIS allowed remote sensing studies to

80 pick out the individual contributions, dynamics and chronologies of dust emission

81 from the mosaic of geomorphic settings and surface types within large basins.

82 MODIS' resolution proved highly appropriate for producing inventories of dust point

83 sources within larger dust source regions (e.g. Bullard *et al.*, 2008; Zhang *et al.*,

84 2008; Lee *et al.*, 2009, 2012; Walker *et al.*, 2009; Baddock *et al.*, 2011; Vickery *et*

85 *al.*, 2013; Hahnenberger and Nicoll, 2014; Kandakji *et al.*, 2020). The hyperspectral

86 capacity of MODIS additionally allowed the development of a range of image

87 processing algorithms (e.g. Ackerman, 1997; Miller, 2003; Murray *et al.*, 2016; Yue

88 *et al.*, 2017) and derived data products (e.g. 'Deep Blue Aerosol Optical Depth' (Hsu

89 *et al*., 2013) and 'Dust Optical Depth' (Ginoux *et al*., 2010)). These approaches have

90 enhanced detection and quantification of suspended dust via its optical and physical

91 properties, and proved useful in the determination of emitting surfaces (e.g. Baddock

92 *et al*., 2015; Yue *et al*., 2017).

93

94 MODIS' spatial resolution in particular has contributed to quantifying and refining of

95 the idea that dust emission is spatially-localized, displaying a 'hotspot' nature, from

96 preferential source areas within a broader landscape (Gillette, 1999). Remote

97 sensing at the sub-basin scale has revealed long term connections between

98 hydrology and geomorphology (both controlling sediment supply and availability),

99 and allowed quantification of different surfaces' potential for dust emission (Kocurek

100 and Lancaster, 1999; Bullard *et al*., 2011). A frequent goal of the sub-basin, MODIS-

101 led studies has been to understand spatial variations in dust emissivity to better

102 represent surfaces in models, toward improved estimates of predicted emission

103 (Zender *et al*., 2003; Bullard *et al*., 2011; Parajuli *et al*., 2014; Baddock *et al*., 2016;

104 Parajuli and Zender, 2017).

105

106 *1.2 New opportunities for observing dust emission at the sub-basin scale*

107 The scale at which MODIS provides insights for characterising preferential dust

108 sources is exemplified in Figure 1. The Chihuahuan Desert of North America was

109 broadly identified as a dust source region by TOMS-based global surveys (Prospero

110 *et al*., 2002), and subsequently, moderate resolution data (AVHRR, Advanced Very

111 High Resolution Radiometer, Rivera Rivera *et al*., 2010; MODIS, Baddock *et al*.,

112 2011; 2016) were applied to elucidate the patterns of dust emission at a sub-basin

113 scale. For instance, in the northern Chihuahuan Desert, both the long term

114 distribution of dust-related satellite data products (processed to 10 km resolution)

115 (Figure 1a) and multi-annual dust event plume analysis (Figure 1b,c) from MODIS

116 have characterised the linkages between dust emission and surface geomorphology

117 in the region. These approaches have highlighted the significance of ephemeral lake

118 and low-relief alluvial systems as preferential sources.

119 <<Figure 1>>

120 Despite insights provided by moderate resolution sensors, the scale of these data
121 means that processes driving dust uplift, operating as surface-boundary layer
122 interactions, can only be inferred (Webb and Strong, 2011). At the level of detail
123 provided by moderate resolution imagers, the heterogeneity in remotely sensed dust
124 observations is largely a product of sensor spatial resolution. It therefore remains
125 difficult to reconcile this resolution with field-based *in situ* investigations of emission
126 which have revealed sub-MODIS-scale variations between eroding and non-eroding
127 surfaces (Lee *et al.*, 2009; Bryant, 2013; Sweeney *et al.*, 2011; von Holdt *et al.*,
128 2019; Cui *et al.*, 2019).

129 In Earth observation for environmental monitoring, fundamental trade-offs exist
130 between spatial and temporal resolutions in the repeat viewing of fixed locations
131 (Cooley *et al.*, 2017). Single platforms with sensors that achieve relatively high
132 resolution surface imaging are usually associated with longer intervals between
133 repeat coverage, such that their sampling prevents frequent observation of dust
134 source activity (e.g. Landsat 8 at 0.03 km offering 16 day repeat in sub-tropical
135 regions). Sensor technologies with off-nadir capabilities such as Satellite Pour
136 l'Observation de la Terre (SPOT; revisit of 1-3 days in this mode) are often utilised
137 for faster emergency response (e.g. Lui and Hodgson, 2016), but are not currently
138 widely available nor archived with global coverage (d'Angelo *et al.*, 2016). The
139 critical importance of temporal sampling explains why daily-to-sub-daily observations
140 from MODIS, and the even higher frequency data capture of the Spinning Enhanced
141 Visible and Infrared instrument (SEVIRI) onboard the geostationary Meteosat
142 Second Generation platform, have proved especially valuable in recording variations
143 in global (Ginoux *et al.*, 2012) and regional dust activity (Schepanski *et al.*, 2007,
144 2009, 2012; Walker *et al.*, 2009; Ashpole and Washington, 2013; Murray *et al.*,
145 2016; Hennen *et al.*, 2019), across moderate/coarse ground resolutions (0.25-10
146 km). New geostationary satellite platforms such as Himawari and GOES-R (~10 min
147 sample time) have significantly improved dust source detection in regions beyond
148 the Sahara (She *et al.*, 2018; Kondragunta *et al.*, 2018). However, the coarse spatial

149 resolution (~2 km) of these sensors is insufficient for pinpointing local sources and

150 detailed observation of dust emission processes (Sowden *et al.*, 2018). Clearly,

151 spatial resolution remains a key constraint for remotely observing, characterising

152 and quantifying dust source behaviour.

153 Where Landsat is a single platform, and MODIS monitors from two satellite platforms

154 (Terra and Aqua, with VIIRS (Visible Infrared Imaging Radiometer Suite) as a

155 comparable afternoon follow-on), recent developments have led to development of

156 miniaturised, multi-platform satellite constellations (e.g. da Silva Curiel *et al.*, 2005)

157 now often referred to as "CubeSats" or "NanoSats". With these constellations,

158 extremely high spatial resolution (0.003-0.005 km) Earth observation is now

159 achievable on a daily or better basis, through coverage achieved by the large

160 number of platforms (Plekhov and Levine, 2018). CubeSat and NanoSat deployment

161 has moved rapidly in Earth observation over the last five years (e.g. Villela *et al.*,

162 2018; Crusan and Galica, 2019) and Planet Lab's suite of Dove satellites equipped

163 with the PlanetScope sensor is one such novel constellation. Systematic

164 interrogation of its finely-resolved spatial data now can provide insights into dust

165 sources at very high resolution (0.002-0.005 km). Given the number of satellites in

166 the PlanetScope constellation, depending on orbits, multiple images can be

167 available for the same location for a given day, providing potential sub-daily,

168 optimally sub-hourly, imaging capability (Plekhov and Levine, 2018). The short (<24

169 h) turnover between PlanetScope data capture and availability for download and

170 processing is an added benefit for dust monitoring, analogous to the near real-time

171 availability of MODIS data.

172 At time of submission, >100 3U CubeSat/Dove platforms (assigned via constellation

173 Flocks; Kopacz *et al.*, 2020) were in orbit, each mounted with the PlanetScope

174 instrument (Planet Labs, 2020), imaging in four bands (Red, Green, Blue, Near-

175 Infrared) with an orthorectified spatial resolution of ~3 m. Regular data from these

176 satellites became available in early 2017, and with its frequent delivery of very high

177 spatial resolution imagery, PlanetScope has been applied in a range of dynamic

178 surface change studies (e.g. Cooley *et al.*, 2017; Wikacsono and Lazuardi, 2018:

179 Park *et al.*, 2019). Given the progress achieved through improved sensor resolution,
180 application of PlanetScope to observing dust sources represents a next step in
181 remote sensing of mineral dust emission.

182 An inherent trade-off in sensor miniaturisation and payload optimisation for systems
183 like PlanetScope, however, concerns the wavelengths sampled, such that
184 PlanetScope provides only four proprietary wavebands. This relatively narrow
185 spectral resolution reduces the opportunities for optimising dust detection afforded
186 by a wider sampled spectral range, and in this paper, simple true-colour scenes are
187 inspected. Despite an absence of multispectral dust enhancement procedures, and
188 issues of subjectivity or inaccuracy in point mapping (Baddock et al., 2009; Walker *et*
189 *al.*, 2009; Sinclair and Legrand, 2019), identifying dust plume origin points with true-
190 colour imagery is an established means of mapping actively emitting portions of
191 surfaces (e.g. Eckardt and Kuring, 2005; Lee *et al.*, 2009; Hahnenberger and Nicoll,
192 2014; O'Loingsigh *et al.*, 2015; Li *et al.*, 2018; Nicoll *et al.*, 2020). PlanetScope data
193 are clearly well-suited for this purpose.

194

1.3 The potential of CubeSats for dust source identification: a case study

196 Herein we demonstrate the potential for understanding dust source characteristics
197 that comes from enhanced satellite spatial resolution, specifically that provided by
198 PlanetScope. We then go on to consider the place of these new data for improved
199 characterisation of dust source dynamics. Our demonstration is used to consider
200 how the capabilities of CubeSats and sensors like PlanetScope occupy a valuable
201 niche in terms of the temporal and spatial constraints limiting remote sensing
202 systems currently applied to dust observation. In a proof-of-concept study, we
203 illustrate the performance of PlanetScope during a dust event occurring in one of
204 North America's most persistent dust sources, presenting this in the wider context of
205 insights that moderate resolution remote sensing provides for source areas in the
206 region. We demonstrate the fact that PlanetScope now offers a spatial fidelity that

207 improves remote detection of dust emission, and can closely augment field-scale
208 observations of dust.

209

210 2. METHOD

211 *2.1 Study location*

212 To demonstrate the potential of high resolution imagery, an example from the
213 northern Chihuahuan Desert is employed. The atmospheric dust loading from the
214 Chihuahuan Desert and the region's importance for aeolian processes in the
215 Western Hemisphere emerged in global remote sensing dust studies (Prospero *et*
216 *al.*, 2002; Ginoux *et al.*, 2012). Further regionally specific studies have helped
217 elucidate the erosivity and erodibility-related controls governing the dust activity (e.g.
218 Lee *et al.*, 2009; Rivera Rivera *et al.*, 2010; Floyd and Gill, 2011; Baddock *et al.*,
219 2011, 2016; Klose *et al.*, 2019) (Figure 1).

220

221 We focus on the Paleolake Palomas (PLP) basin, an extensive Pleistocene pluvial
222 lake system spanning the present-day boundaries of Chihuahua (Mexico) and New
223 Mexico (USA), which covered ~7700 km^2 at maximum extent (Dominguez Acosta,
224 2009). The basin now exists as a series of interconnected ephemerally-inundated
225 playas (Castiglia and Fawcett, 2006) which serve as dust emission hotspots
226 (Dominguez Acosta, 2009; Rivera Rivera *et al.*, 2010; Baddock *et al.*, 2011, 2016).
227 The largest and southernmost of these playas, Bolson de los Muertos (BdlM),
228 extends approximately 90 km north-south and up to 25 km east-west at its widest
229 point. The BdlM consists of a wide central "body" with two "arms" (lobes) extending
230 to the southwest and southeast (Figure 1c). Each lobe is associated with an
231 inputting river system that no longer enters the BdlM under contemporary conditions
232 but was connected during late Pleistocene wet periods (Rio Santa Maria entering the
233 SW lobe and Rio del Carmen the SE lobe) (Dominguez Acosta, 2009). Historical
234 fluvial inputs associated with the discharge of the Rio Santa Maria into the SW lobe
235 led to the deposition of deltaic sediments in portions of the playa (marked on Figure
236 1c).

237

238   While lacking regular fluvial inflow in the present climate, the two individual lobes
239   occasionally demonstrate "wet playa" behaviour (Rosen, 1994) associated with their
240   status as regional topographical sinks. Acting as small endorheic basins, the lobes
241   periodically accumulate water from major regional precipitation events, receiving in-
242   washed alluvial sediment from surrounding higher elevations. This hydrological and
243   sediment recharge behaviour modulates the lobes' activity as sources of dust, but
244   contributes to the overall highly emissive nature of these playa surfaces in the longer
245   term (Reynolds *et al.*, 2007) (Figure 1a,b).

246

247   For this case study, we consider the southwestern arm of the BdlM (SW BdlM),
248   elongating approximately 30 km in a NNE direction and 9 km wide. The inner part of
249   the SW BdlM is generally unvegetated, flat, devoid of non-erodible elements, and
250   filled with fine (silty clay) clastic sediments, covered after evaporation of late summer
251   monsoon moisture by a thin clay crust. Surrounding this inner core of playa
252   sediments is a sparsely-vegetated (a few patches of grasses) marginal sand sheet
253   augmented with fluvial-deltaic sediments to the northwest, deposited by the paleo-
254   inflows of the Rio Santa Maria, and Quaternary alluvial deposits on the west, shed
255   from the Cerros la Nopalera. These fluvial and alluvial sediments accumulated on
256   the western and northern SW BdlM playa surfaces as graded beds ranging from clay
257   and silts to small amounts of sand-sized sediments and some deltaic rounded
258   gravels (Dominguez Acosta, 2009). Land use is very sparse and primarily livestock
259   grazing, although irrigated cropland agriculture is practiced in isolated areas
260   adjoining the BdlM and more widely in the floodplain of the modern Rio Santa Maria
261   upstream. There is minimal land use of the playa surface itself.

262

263   The combination of strong westerly/southwesterly winds (perpendicular to the
264   orientation of the PLP basin) during the dry season, and sands on the upwind outer
265   margin of the playa that saltate onto the fine sediments in the playa's centre, leads
266   to frequent emission of dust plumes from the BdlM. Such events are regularly
267   identifiable on MODIS imagery (Lee *et al.*, 2009; Rivera Rivera *et al.*, 2010; Baddock
268   *et al.*, 2011) (Figure 1b,c). Dust plumes from the BdlM, other sub-basins of PLP, and

269   other sources regularly merge into regional-scale dust events which cause air quality

270   hazards to the Ciudad Juarez (Chihuahua)-El Paso (Texas) metropolitan area

271   (Rivera Rivera *et al.*, 2010; Rivas *et al.*, 2019) and can extend at least 800 km

272   downwind across Texas (Lee *et al.*, 2009).

273

274   Previous research has examined Chihuahuan Desert dust sources at a sub-basin

275   scale, using the Preferential Dust Source (PDS) classification scheme (Baddock *et*

276   *al.,* 2011; Bullard *et al.*, 2011). PDS was designed to represent observations that

277   dust-yielding basins are comprised of different geomorphology or surface types,

278   each with varying potentials to emit dust. The PDS surface classification effort was

279   intended to understand the influence of variations in surfaces and their sediments on

280   dust activity at a sub-basin scale (Bullard *et al.*, 2011). The PDS scheme was

281   applied to the Chihuahuan Desert (e.g. Figure 1b), and is explained, by Baddock *et*

282   *al.* (2011), who mapped attribution of PDS geomorphological classes to polygons of

283   the Mexican national land type mapping system ("Sistema de Topoformas") as

284   distributed by the national geospatial agency (INEGI, 2001). For the smaller scale of

285   the current SW BdlM study, it was possible to use the more detailed national soil

286   map polygons provided by INEGI (2001).

287

288   To help formalise the analysis of the dust event, a regular grid of 100 m^2 cells was

289   generated over the polygon from the PDS scheme representing the entire BdlM

290   (Figure 1c). While application of this 100 m scale grid is somewhat arbitrary, in their

291   review of wind erosion modelling, Webb and Strong (2011) propose the scale

292   between what they term 'plot' (10^1) and 'landscape' (10^3) as the appropriate scale at

293   which to consider emission processes. Analysing these 100 m cells is an appropriate

294   scale to map emission detectable in (~3 m resolution) PlanetScope imagery.

295

296   *2.2 Study dust event and satellite imagery*

297   To illustrate a dust event detected via high resolution PlanetScope in the context of

298   moderately resolved MODIS data for the region (Figure 1), dust emission occurring

299   at the SW BdlM was chosen from 30th November 2018. On this day, a strong Pacific

300 cold front, aligned with an upper-level trough and extending southwestward from a
301 cyclone centred in northeast New Mexico, crossed the northern Chihuahuan Desert
302 from west to east. This produces an ideal synoptic weather pattern for dust storms in
303 the region (Rivera Rivera *et al.*, 2009). Winds gusted to 90 km/h at El Paso
304 International Airport, ~140 km north-northeast of the SW BdlM; hourly PM_{10}
305 concentration recorded by the Texas Commission on Environmental Quality at
306 Socorro (southeast of El Paso and ~130 km northeast of the SW BdlM) reached 961
307 $\mu g/m^3$ while hourly $PM_{2.5}$ concentration reached 62 $\mu g/m^3$, both at 0900 MST (1600
308 UTC).

309

310 Imagery for the event was obtained from the Planet Labs exploration portal
311 (www.planet.com) and the NASA Worldview site for pre-processed MODIS data. We
312 examine true-colour imagery of SW BdlM from PlanetScope (1706 UTC capture
313 time), and MODIS Terra (1735 UTC) and Aqua (2050 UTC). For PlanetScope,
314 bands 1-3 (Blue: 455-515 nm, Green: 500-590, Red: 590-670 nm) of the Level 3B
315 Analytic Ortho Scene Product in GeoTIFF format were obtained and composited to
316 produce simple true-colour scenes. Two scenes from 1706 UTC imaged along the
317 same sensor overpass (37 and 38 seconds past the minute) were used in a mosaic
318 over the SW BdlM study area.

319

320 3. RESULTS

321 A broad view of the 30th November 2018 BdlM dust event is shown by the Terra and
322 Aqua MODIS scenes (Figure 2a,b). MODIS imagery quality for the event is relatively
323 poor, due to inherent problems of native resolution (WorldView imagery resampled
324 to 250 m) and pixel stretch near the edge of the image swath, but the MODIS true-
325 colour data reveal dust in a part of the playa known to emit often. In the Aqua scene,
326 an elevated plume is most clearly visible heading eastward, showing a typical dust
327 uplift pattern with the passage of a Pacific cold front (cf. Figure 1c). A best-estimate
328 of the upwind point of the plumes identifies active emission in the SW BdlM, which
329 the long term point source inventory indicates is an area prone to emission (Figure
330 1b).

331

332 PlanetScope overpasses covering the event were available from ~30 minutes before

333 the Terra overpass. Analysis of the PlanetScope data reveals numerous discrete,

334 identifiable dust plumes in the SW BdlM, whose upwind extent can be tracked to

335 specific emitting parts of the playa surface (Figure 2c [A high resolution image of this

336 figure panel is available in the Supplementary Material]). Directly comparing the best

337 interpretation of the true-colour MODIS and PlanetScope scenes, the MODIS points

338 coincide fairly well with the most well-developed coalesced plumes shown on

339 PlanetScope, <2 km of their apparent upwind origins (Figure 2d). Crucially however,

340 many more smaller plumes are identifiable via PlanetScope from multiple parts of

341 the playa, providing much more detail and accuracy concerning the specific parts of

342 the surface that are emitting.

343

344 When applied to the regular 100 m^2 grid placed over the BdlM, those grid cells

345 where emission and plume initiation could unambiguously be identified at the upwind

346 edge of the lofted plumes are highlighted (Figure 2d). The area of focus indicated in

347 Figure 2a,b represents an approximately 8.25 km square section (68.3 km^2). Image

348 interpretation indicates that 68 cells contained the onset of plumes at the upwind

349 boundaries of emission (Figure 2d), equating to ~1% of the focus area. MODIS-

350 based studies have identified a significant bias in favour of identification of upwind

351 source points in point inventories (e.g. Lee *et al.*, 2009; 2012; also SEVIRI, Hennen

352 *et al.*, 2019), due to the inability to detect discrete points invisible underneath the

353 main plume. This limitation largely restricts determination of source points to those at

354 the upwind "plume heads" (Walker *et al.*, 2009; Sinclair and Legrand, 2019). Whilst

355 also an issue for interpretation of the PlanetScope imagery, the increased level of

356 detail from PlanetScope offers increased ability to ascertain those surfaces that are

357 actively emitting downwind from the upwind boundary of emission. In Figure 2d,

358 additional cells estimated as being highly likely to contain emission, as evidenced by

359 the presence of multiple plumes appearing close to the surface, and downwind of

360 discernible upwind initiation, are also indicated. These additional 499 cells account

361 for a further ~7.3% of the area, indicating evidence of dust emission occurring in

362 total over ~8% of the focus portion of SW BdlM.

363

364 4. DISCUSSION

365 *4.1 Pinpointing dust point source locations and geomorphology from high resolution*

366 *imagery*

367 Here, in showing PlanetScope imagery over a source area during a dust emission

368 event, we demonstrate how its high resolution allows direct observation of active

369 plume development to an unprecedented degree. That the imagery allows

370 pinpointing of the upwind origin of individual dust plumes to precise emission

371 surfaces and small-scale geomorphic setting emphasises the detail of emission

372 processes that can be unlocked from these high resolution images. This capability

373 achieves insights into the spatial heterogeneity of processes and emission far

374 beyond that revealed by moderate resolution sensing (Figure 1; Figure 2).

375

376 For instance, PlanetScope reveals that the cluster of dust plumes initiating from the

377 outer northwest portion of the BdlM focus area (Figure 2c,d) is located in a zone

378 where numerous small washes terminate, indicating where sediments of mixed sizes

379 from the Rio Santa Maria paleodelta are likely to have been brought onto the playa.

380 This line of washes and presence of fluvial material extends to the northeast, with

381 the distribution of active dust emission grid cells also stretched in that direction. This

382 location is also consistent with areas where playa-marginal sands, undergoing

383 saltation by W-WSW wind, would move onto lacustrine clays dominating the inner

384 playa surface. Such contact zones in playa basins are well known to become

385 preferential dust sources due to the combination of loose sands for saltation

386 bombardment over fine sediments (Cahill *et al.*, 1996; Gill, 1996; Lee *et al.*, 2009;

387 Rivera Rivera *et al.*, 2010; Bullard *et al.*, 2011).

388

389 The multiple dust plumes in the central part of the playa shown by PlanetScope,

390 close to the source point evident from Aqua MODIS, also reveal emission occurring

391   further from the edges and availability of aeolian or fluvial inputs, which potentially

392   reflects the action of other emission drivers (Figure 2d). Dust emission here may be

393   associated with areas of weakly-crusted playa surface, susceptible to breakage and

394   auto-erosion, exposing unconsolidated silt-clay sediments underneath to the wind,

395   as documented on other parts of the BdlM (Dominguez Acosta, 2009) and at Owens

396   Lake (Cahill *et al.*, 1996). The most southerly cluster of dust plumes revealed by

397   PlanetScope in the scene is again consistent with W‑WSW winds entraining sand

398   sheet sediments from the upwind outer playa, bringing them into contact with finer

399   lacustrine clays and silts, to drive dust emission. In addition, the long fetch in the

400   direction of wind run across the flat playa likely contributes to a high potential for

401   emission from erodible surfaces downwind (Cahill *et al.*, 1996; Gillette, 1999).

402   Clearly, the detail in which aeolian processes can be interpreted from PlanetScope

403   is much improved over the equivalent MODIS data. Although Figure 2d indicates

404   broad spatial agreement between the MODIS-estimated plume origins and the

405   pinpoint distribution from PlanetScope, an enhanced ability to interpret processes

406   stems from improved accuracy in determination of emission points in high resolution

407   data (Sinclair and Legrand, 2019). In source identification studies led by moderate

408   resolution sensors with daily sampling rate, uncertainty can exist whether the upwind

409   edge of a plume is associated with active emission at the time of capture

410   (Schepanski et al., 2007; 2009). Here, when PlanetScope overpass clearly occurs

411   some time after the onset of emission, the detail of scene resolution allows plumes

412   to be unambiguously traced back to ongoing, active emission (Figure 2c).

413

414   A comparable dust-free scene of the SW BdlM from a few days before the study

415   event, is valuable for characterising contemporary surface state, and its temporal

416   change, in a system such as a playa (Figure 3) (Reynolds *et al.*, 2007; Urban *et al.*,

417   2018). For instance, PlanetScope detail in the dust-free image is sufficient to identify

418   large polygon-shaped desiccation peds (characteristic of the BdlM in general

419   (Dominguez Acosta, 2009)), indicating the high clay and silt concentrations, and

420   surfaces previously inundated by water. Figure 3 also specifically indicates dust was

421   not emitted from the central portion of the focus area, where the surface appears

422 visibly darker. This darker surface indicates the presence of vegetation at the time,

423 as evidenced by comparison of vegetated channels and arroyos seen off the playa,

424 most notably to the west. Where vegetation likely to be of remnant state acts as non-

425 erodible cover on the central portion of the playa saltation bombardment will be

426 impeded (Lancaster and Baas, 1998), thus limiting plume development. Inspection

427 of the dust-free imagery helps to account for this control on emission.

428 << Figure 3 >>

429

430 In summary, the detail provided by the PlanetScope imaging of plume sources

431 reinforces the broader importance for dust emission of contacts between different

432 geomorphic domains. In this case, the known connectivity between saltator

433 availability at playa margins, fluvially-provided wind-suspendible fines, and lacustrine

434 sediment of variably crusted state is emphasised for the first time in satellite

435 imagery. These and other linkages can be determined by interpretating the locations

436 where emission points can be unambiguously pinpointed (Mahowald *et al.*, 2003;

437 Lee *et al.*, 2009; Bullard *et al.*, 2011; Klose *et al.*, 2019).

438

439 *4.2 Scale limits for dust source monitoring using PlanetScope data*

440 In order to understand dust emission processes, one of the key challenges has been

441 to match remote sensing observations to the space and time scales of field-

442 observed emission (Bullard, 2010; Bryant, 2013). The BdlM dust source

443 observations in our case study enable reflection on the relative contribution of

444 remote sensing data to both dust source and dust plume detection, and how these

445 relate to improved understanding of emission. The relative scales at which

446 commonly used remote sensing data are able to characterise dust emission events

447 are summarised in Figure 4. When considering these, a number of studies

448 acknowledge the small scale and stochastic nature of the dust emission process

449 (e.g. Gillette, 1999; Lee *et a*l., 2009; Bullard *et al.*, 2011; Shao *et al.,* 2011; Kok *et*

450 *al.*, 2014). Field and modelling studies in and around playa basins (e.g. Cahill *et al.*,

451 1996; King *et al.*, 2011; Sweeney *et al.*, 2011; von Holdt *et al.*, 2019) have

452 highlighted the variability of surface erodibility and the importance of crusts for the

453 dust emission process. Haustein *et al.* (2015) go one step further, matching the

454 scale of emission to dust modelling schemes, highlighting how surface heterogeneity

455 can lead to significant uncertainty in model estimates. Using the most informative

456 studies in terms of the spatial scale of emissions, such as Webb and Strong (2011)

457 and Haustein *et al.* (2015) as a baseline, we infer an approximate "scale limit" (c. 10^2

458 m and <1 day) for dust source detection that is able to capture site information

459 appropriate to the scale of surface erodibility heterogeneity. This is the scale that

460 can be complementary to *in situ* observation of emission. For understanding the

461 contribution of remote sensing, this "scale limit" therefore represents an arbitrary

462 divider between remote sensing detection of dust emissions observed at the field-

463 scale (thereby linked to process), and dust plumes evident at the basin and sub-

464 basin scale (from which we must infer process). Temporally, it is clear that

465 observations captured sub-daily are also essential to establish the locations of dust

466 emission (Schepanski et al., 2009; Shao *et al.*, 2011; Webb *et al.,* 2019; Klose *et al.*,

467 2019); such observations are possible with the PlanetScope data (Figure 5).

468

469 <<Figure 4>>

470 <<Figure 5>>

471

472 Webb and Strong (2011) provide a robust framework for the spatial and temporal

473 scales at which dust emission and transport operate. A summary of how these

474 processes are sampled by remote sensing data types is provided in Figure 4, and

475 we use our emission scale limit to consider the likely detection of dust in transport,

476 or, dust emission at source. In terms of temporal resolution, we note that the

477 frequency of dust event detection (e.g. as observed from synoptic weather code

478 reports at WMO sites; O'Loingsigh *et al.*, 2010) increases significantly at a sub-day

479 frequency (e.g. Novlan *et al.* (2007) for the northern Chihuahuan Desert). Figure 4

480 shows that most current dust remote sensing applications work outside the required

481 lower scale limit. Initial source detection efforts using TOMS (e.g. Prospero *et al.*,

482 2002; Figure 4, A) were only able to identify candidate basin-scale dust sources and

483 subsequently relate the dynamics of these to regional climate and landscape scale

484 processes (e.g. Bryant *et al.*, 2007). At a basin and sub-basin scale, geostationary

485 satellites (e.g. SEVIRI: Schmetz *et al.*, 2002; Himawari: Bessho *et al.*, 2016) have

486 been used to detect, track and characterise dust emissions over large regions (e.g.

487 Schepanski et al., 2009; Banks and Brindley, 2013; Figure 4, B). In practice, these

488 data have been used to (i) detect and build inventories of dust events used to infer

489 source regions (e.g. Hennen *et al.*, 2019), (ii) match events to synchronous data to

490 determine climatological drivers of emission over short (<day) to decadal timescales

491 (e.g. Schepanski et al., 2009; Gasch *et al.*, 2017), and (iii) provide quantitative

492 estimates of dust properties and radiative impacts (e.g. Brindley *et al.*, 2012). Where

493 these data have been used to detect and identify dust events at the sub-basin scale

494 (e.g. Murray *et al.*, 2016; Hennen *et al.*, 2019) they are often only able to track

495 clearly visible plumes locations to within 3-8 km of likely source location, making

496 links between plot-scale emission processes and dust events difficult to resolve

497 (Figure 4, B).

498

499 Data from moderate resolution sensors (e.g. MODIS, VIIRS; Figure 4, C), have also

500 been used extensively to observe plumes close to dust sources either involving

501 subjective analyses (e.g. Bullard *et al.*, 2008; Baddock *et al.*, 2009; Lee *et al.,* 2009;

502 2012) or the use of processed, dust-related data products (e.g. Ginoux *et al.*, 2010;

503 2012; Baddock *et al.*, 2016). The increased spatial resolution of MODIS-like data

504 produces a shift towards the suggested scale limit, thereby enhancing

505 characterisation of dust emission hot spots and their candidate geomorphic settings.

506 Synergistic use of data from these moderate resolution sensors has also increased

507 our understanding of dust sources and transport corridors (e.g. Bakker *et al.,* 2019).

508 As an Earth monitoring system, the combination of Sentinel 2A/B and Landsat 8

509 (Figure 4, D) offers the ability to determine dust emission at a scale which may

510 approach the required scale limit. The image resolution and image scene size of

511 these data certainly facilitate dust plume interpretation at the sub-basin and landform

512 scale (e.g. von Holdt *et al.*, 2017; 2019), however, the best combined revisit period

513 for these data for most areas (c. 5 days) still falls below that required to capture dust

514 emission data sufficiently regularly to usefully match field observations (e.g. Li and

515 Roy, 2017). In our case study, we show the relative advance that PlanetScope data,

516 and CubeSat-constellation observation systems in general, can make through high

517 spatial and temporal observation of dust source dynamics, operating *inside* the

518 suggested space/time scale limits for plot-scale monitoring proposed here (Figure 4,

519 E).

520

521 4.3 *Benefits of dust emission monitoring via CubeSats*

522 The analysis provided in Figure 2 indicates how future in-depth studies might

523 characterise specific emission locations with greater space/time fidelity than can

524 moderate resolution sensors, and thereby may better inform representation of

525 surface types within dust emission models. Dust emission characterisation through

526 PlanetScope's high resolution imagery is clearly relevant to the small scale

527 parameterisations required to improve large-scale dust modelling (Thomas and

528 Wiggs, 2008; Bullard, 2010). Within an area of land surface known to be highly

529 emissive, in this example <10% of the surface was assessed to be unambiguously

530 emitting at one time during the study dust event (Figure 2d). At the scale of the PDS

531 classification, the whole of BdlM is uniformly classified as "ephemeral playa" (class

532 1b; Bullard *et al.,* 2011). PlanetScope, however, establishes the actual spatial

533 variability of emission within this single MODIS-scale surface class, helping to

534 account for variability in emission potential observable in the field (e.g. von Holdt *et*

535 *al.*, 2019; Klose *et al.*, 2019; Cui *et al.*, 2019).

536

537 Another key benefit of high resolution monitoring of aeolian processes is an

538 improved ability to constrain timing of dust uplift and the role of small-scale

539 meteorological processes in dust emission, approaching comparability with field-

540 based observations (Figure 5). The contribution of high temporal frequency remote

541 sensing in this regard has been demonstrated for SEVIRI (e.g. Schepanski *et al.*,

542 2009). Future studies that couple high spatial resolution imaging with high temporal

543 resolution ground-based measurement of key meteorological variables (the latter

544 primarily related to determining transport capacity i.e. shear velocity, turbulent

545 gusting etc.), will combine "top down" and "bottom up" perspectives of dust emission

546 (Richter and Gill, 2018) with better fidelity. Detailed ground observation studies such

547 as the intensive remote camera-based dust monitoring of Soda Lake, a Mojave

548 Desert playa, by Urban *et al.* (2018), are one way to evaluate the level of dust

549 activity that PlanetScope can additionally retrieve.

550

551 Aside from the transport capacity-limitation (wind threshold exceedance), dust uplift

552 in most global dust source areas is also limited by two other factors; (i) sediment

553 availability, and/or (ii) sediment supply (Kocurek and Lancaster, 1999; Bullard *et al.*,

554 2011). When considering the sediment availability-limitation, the temporary flooding

555 of a surface, such as the BdlM playa, often followed by vegetation growth and/or

556 development of surface crusting, leads to dust-sized sediment not being available to

557 erode. After drying or crust weakening, this availability-limitation becomes relaxed,

558 and sources may emit again (Mahowald *et al.*, 2003; Bryant *et al.*, 2007). Periodic

559 'switching off-switching on' of dust emission is a fundamental aspect of variability in

560 dust source activity, and must be accounted for in the accurate simulation of regional

561 dust regimes. Detailed imagery such as from PlanetScope will enable daily

562 monitoring of emissions from specific surfaces, revealing both when and where they

563 begin to be emissive, and crucially, when and where they do *not*. While timing of

564 overpasses will remain an issue for capture of emission, the repeat spatial resolution

565 of CubeSats can nevertheless better establish controls on (i) geomorphic thresholds

566 of emission, and (ii) temporal constraints on dust uplift. In the latter case, linkage of

567 pinpoint emission observation to key meteorological parameters, including *in situ*

568 measurements where possible (e.g. Haustein *et al.*, 2015), and to hydrological

569 histories of the location (inundation and drought regime), can help validate dust

570 modelling efforts.

571

572 Finally, we suggest how the unprecedented detail of CubeSat data can guide

573 enquiry into dust emission for both future remote sensing technologies and field

574 observations. For instance, one important contribution will be the opportunity to help

575 target remote sensing missions such as the Earth Surface Mineral Dust Source

576 Investigation (EMIT; Thompson *et al.*, 2020), by providing enhanced understanding

577 of the dynamics of dust emission surfaces (especially crust distribution and types). In

578 terms of field-based measurement of dust flux and/or emission potential of surfaces,

579 von Holdt *et al.* (2017; 2019) demonstrated how the relatively high spatial resolution

580 of Landsat data aided the location of field campaigns to test emissions from different

581 surfaces. The increased space/time precision of source mapping offered by sensors

582 like PlanetScope will be invaluable for guiding field studies designed to quantify dust

583 emission rates from surface types within landscapes (King *et al.*, 2011; Sweeney *et*

584 *al.*, 2011; Bryant, 2013; Klose *et al.*, 2019). Additional to the long term (multi-annual)

585 monitoring of emission surfaces, we note that the rapid delivery of PlanetScope data

586 after collection, and the near real-time provision of imagery, will permit observation

587 of dust events almost as they unfold. Such a facility benefits field studies and other

588 *in situ* observation campaigns such as fixed-point air quality monitoring, and for

589 purposes of fugitive dust identification and wind erosion mitigation (e.g. Miller *et al.*,

590 2012; Kandakji *et al.*, 2020).

591

592 4.4. *Some limitations of CubeSat data for dust source observation*

593 In terms of their application to observing dust within source areas, some limitations

594 of CubeSat and the PlanetScope data used here specifically, require noting.

595 Considering the role of CubeSats for observing dynamic surface change

596 phenomena, Cooley *et al.* (2017) emphasise that constellation-derived imagery is

597 acquired by way of smaller, lower budget sensors such that radiometric quality,

598 consistency and signal-to-noise ratios are below that of missions supported by major

599 space agencies. The large number of individual platforms comprising any

600 constellation unavoidably produces inconsistency about cross-sensor calibration,

601 image quality and accuracy of geolocation, all of which represent general limitations.

602 For PlanetScope geolocation error is reported <10 m (Planet Labs, 2020), but given

603 the scale at which dust emission can be considered, any such inaccuracy was

604 effectively mitigated within the 100 m grid source cell approach adopted here.

605 With the high albedo caused by often limited vegetation and typically light-coloured

606 sediments in dust source areas, many sources are characterised by bright surfaces

607 which can confound observation of plumes using only visible bands (Kaufman *et al.*,

608 2002; Miller, 2003; Zhang *et al.*, 2008). With only one non-visible band, opportunities

609 for algorithmic enhancement of dust in PlanetScope data are limited. While

610 recognising this issue, in this study we focused on interpretation of basic true-colour

611 scenes, and as we demonstrate, problems of plume definition are mitigated to some

612 extent by the excellent spatial resolution. CubeSat sensors may be especially prone

613 to signal saturation over bright surfaces, precluding plume detection in the worst

614 cases. This point, however, should be regarded next to the issue that dust detection

615 over bright surfaces can be problematic even for multi-spectral sensors such as

616 MODIS and SEVIRI (Baddock *et al.*, 2009; Schepanski *et al.*, 2009). 'Clear sky

617 differencing', where dust-free images are subtracted to emphasise the presence of

618 dust has proven a fruitful approach (Murray *et al.,* 2016). The regular repeat viewing

619 provided by CubeSats means that recent clean scenes required for background

620 subtraction should be readily available (Figure 3). This facilitates clear sky

621 differencing as a straightforward way to potentially enhance the appearance of dust

622 plumes from CubeSat imagery. The presence of cloud is a known complication for

623 remote methods of dust detection (Ackerman, 1997; Miller, 2003; Baddock *et al.*,

624 2009), and the absence of any inherent cloud masking processing for CubeSat data

625 increases the need for user interpretation of scenes (Cooley *et al.*, 2017).

626

5 CONCLUSION

628 Advances in the spatial and temporal resolution of terrestrial remote sensing over

629 the past two decades have revealed the sources of aeolian dust with improving

630 spatial and temporal fidelity. Our case study suffices to show that the extreme spatial

631 detail, coupled with daily/sub-daily global coverage available from CubeSats such as

632 PlanetScope, provides a leap forward in our ability to monitor aeolian dust dynamics

633 through remote sensing. We offer a number of concluding remarks:

634   ● We demonstrate the capabilities and potential benefits for understanding dust

635   source behaviour achievable with highly-spatially-resolved imagery now

636   readily available on a daily basis with global coverage.

637   ● We show that the detail in which dust plumes can be captured with

638   PlanetScope data now allows visualisation of dust emission at a scale which,

639   for the first time, can realistically augment field measurements. The daily

640   availability of data is comparable to moderate resolution sesors, but the

641   opportunity for sub-daily constellation-based CubeSat imaging also provides

642   considerable additional potential. Considering other remote sensing systems

643   currently used for dust source observation, coupling CubeSat performance

644   with hyper-temporal monitoring of dust source activity (e.g. via SEVIRI,

645   GOES-16/17), will significantly enhance our ability to monitor and understand

646   source dynamics.

647   ● Taking advantage of its unprecedented detail and global coverage, we call for

648   future, systematic evaluations of constellation-based, high spatial resolution

649   imagery. These data provide a new impetus for informing our understanding

650   of the spatio-temporal distribution of aeolian processes, the drivers of aeolian

651   processes within the global dust cycle, and their representation in regional

652   and global climate models.

653

654   6 ACKNOWLEDGMENTS

661

662   REFERENCES

663

664 Ackerman, S.A., 1997. Remote sensing aerosols using satellite infrared
665 observations. J. Geophys. Res. 102, 17069–17079.

666

667 Ashpole, I., Washington, R., 2013. A new high-resolution central and western
668 Saharan summertime dust source map from automated satellite dust plume tracking.
669 J. Geophys. Res. 118, 6981-6995.

670

671 Baddock, M.C., Bullard, J.E., Bryant, R.G., 2009. Dust source identification using
672 MODIS: a comparison of techniques applied to the Lake Eyre Basin, Australia.
673 Remote Sens. Environ. 113, 1511–1528.

674

675 Baddock, M.C., Gill, T.E., Bullard, J.E., Dominguez Acosta, M., Rivera Rivera, N.I.,
676 2011. Geomorphology of the Chihuahuan Desert based on potential dust emissions.
677 J. Maps 7, 249–259.

678

679 Baddock, M.C., Parsons, K., Strong, C.L., Leys, J.F., McTainsh, G.H., 2015. Drivers
680 of Australian dust: a case study of frontal winds and dust dynamics in the lower Lake
681 Eyre Basin. Earth Surf. Process. Landf. 40, 982-1988.

682

683 Baddock, M.C., Ginoux, P., Bullard, J.E., Gill, T.E., 2016. Do MODIS-defined dust
684 sources have a geomorphological signature? Geophys. Res. Lett. 43, 2606–2613.

685

686 Bakker, N.L., Drake, N.A., Bristow, C.S., 2019. Evaluating the relative importance of
687 northern African mineral dust sources using remote sensing. Atmos. Chem. Phys.
688 19, 10525-10535.

689

690 Banks, J.R., Brindley, H.E., 2013. Evaluation of MSG-SEVIRI mineral dust retrieval
691 products over North Africa and the Middle East. Remote Sens. Environ. 128, 58-73.

692

693 Bessho, K., Date, K., Hayashi, M., Ikeda, A., Imai, T., Inoue, H., Kumagai, Y.,
694 Miyakawa, T., Murata, H., Ohno, T. and Okuyama, A., 2016. An introduction to
695 Himawari-8/9—Japan's new-generation geostationary meteorological satellites. J.
696 Meteorol. Soc. Japan. Ser. II. 94, 151-183.

697

698 Brindley, H., Knippertz, P., Ryder, C., Ashpole, I., 2013. A critical evaluation of the
699 ability of the Spinning Enhanced Visible and Infrared Imager (SEVIRI) thermal
700 infrared red-green-blue rendering to identify dust events. Theoretical analysis. J
701 Geophys. Res. 117, D07201.

702

703 Bryant, R.G., 2013. Recent advances in our understanding of dust source emission
704 processes. Prog. Phys. Geogr. 37, 397–421.
705

706 Bryant, R.G., Bigg, G.R., Mahowald, N.M., Eckardt, F.D., Ross, S.G., 2007. Dust
707 emission response to climate in southern Africa. J. Geophys. Res. 112, D09207.
708

709 Bullard, J., 2010. Bridging the gap between field data and global models: Current
710 strategies in aeolian research. Earth Surf. Process. Landf., 35, 496–499.
711

712 Bullard, J., Baddock, M., McTainsh, G., Leys, J., 2008. Sub-basin scale dust source
713 geomorphology detected using MODIS. Geophys. Res. Lett., 25, L15404.
714

715 Bullard, J.E., Harrison, S.P., Baddock, M.C., Drake, N., Gill, T.E., McTainsh, G.,
716 Sun, Y., 2011. Preferential dust sources: a geomorphological classification designed
717 for use in global dust-cycle models. J. Geophys. Res. 116, F04034.
718

719 Cahill, T.A., Gill, T.E., Reid, J.S., Gearhart, E.A., Gillette, D.A., 1996. Saltating
720 particles, playa crusts and dust aerosols at Owens (dry) Lake, California. Earth Surf.
721 Process. Landf. 21, 621–639.
722

723 Castiglia, P.J., Fawcett, P.J., 2006. Large Holocene lakes and climate change in the
724 Chihuahuan Desert. Geology 34, 113–116.
725

726 Cooley, S.W., Smith, L.C., Stepan, L., Mascaro, J., 2017. Tracking dynamic northern
727 surface water changes with high-frequency Planet CubeSat imagery. Remote Sens.
728 9, 1306.
729

730 Cui, M., Lu, H., Wiggs, G.F., Etyemezian, V., Sweeney, M.R., Xu, Z., 2019.
731 Quantifying the effect of geomorphology on aeolian dust emission potential in
732 northern China. Earth Surf. Process. Landf. 44, 2872-2884.
733

734 d'Angelo, P., Máttyus, G., Reinartz, P., 2016. Skybox image and video product
735 evaluation. Int. J. Image Data Fus., 7, 3-18.
736

737 da Silva Curiel, A., Boland, L., Cooksley, J., Bekhti, M., Stephens, P., Sun, W.,
738 Sweeting, M., 2005. First results from the disaster monitoring constellation (DMC).
739 Acta Astronaut. 56, 261-271.
740

741 Dominguez Acosta, M., 2009. The Pluvial Lake Palomas-Samalyuca Dunes System.
742 Ph.D. Dissertation (Geological Sciences), University of Texas at El Paso.

743

744 Eckardt, F.D., Kuring, N., 2005. SeaWiFS identifies dust sources in the Namib
745 Desert. Int. J. Rem. Sens. 26, 4159-4167.

746

747 Field, J.P., Breshears, D.D., Whicker, J.J., 2009. Toward a more holistic perspective
748 of soil erosion: Why aeolian research needs to explicitly consider fluvial processes
749 and interactions. Aeolian Res. 1, 9–17.

750

751 Floyd, K.W., Gill, T.E., 2011. The association of land cover with aeolian sediment
752 production at Jornada Basin, New Mexico, USA. Aeolian Res. 3, 55-66.

753

754 Gasch, P., Rieger, D., Walter, C., Khain, P., Levi, Y., Knippertz, P., Vogel, B., 2017.
755 Revealing the meteorological drivers of the September 2015 severe dust event in
756 the Eastern Mediterranean. Atmos. Chem. Phys. 17, 13573-13604.

757

758 Gill, T.E., 1996. Eolian sediments generated by anthropogenic disturbance of playas:
759 human impacts on the geomorphic system and geomorphic impacts on the human
760 system. Geomorphology 17, 207-228.

761

762 Gillette, D.A., 1999. A qualitative geophysical explanation for hot spot dust emitting
763 source regions. Contrib. Atmos. Phys. 72 (1), 67–78.

764

765 Ginoux, P., Garbuzov, D., Hsu, N.C., 2010. Identification of anthropogenic and
766 natural dust sources using Moderate Resolution Imaging Spectroradiometer
767 (MODIS) Deep Blue level 2 data, J. Geophys. Res., 115, D05204.

768

769 Ginoux, P., Prospero, J.M., Gill, T.E., Hsu, N.C., Zhao, M., 2012. Global-scale
770 attribution of anthropogenic and natural dust sources and their emission rates based
771 on MODIS Deep Blue aerosol products. Rev. Geophys. 50, RG3005.

772

773 Hahnenberger, M., Nicoll, K., 2014, Geomorphic and land cover identification of dust
774 sources in the eastern Great Basin of Utah, USA. Geomorphology, 204, 657-672.

775

776 Haustein, K., Washington, R., King, J., Wiggs, G., Thomas, D.S.G., Eckardt, F.D.,
777 Bryant, R.G., Menut, L., 2015. Testing the performance of state-of-the-art dust
778 emission schemes using DO4Models field data. Geosci. Model Dev. 8, 341-362.

779

780 Heinold, B., Tegen, I., Schepanski, K., Banks, J.R., 2016. New developments in the
781 representation of Saharan dust sources in the aerosol-climate model ECHAM6-
782 HAM2. Geosci. Model Dev. 9, 765–777.

783

784 Hennen, M., White, K. Shahgedanova, M., 2019. An assessment of SEVIRI imagery
785 at various temporal resolutions and the effect on accurate dust emission mapping.
786 Remote Sens.11, 918.

787

788 Hsu, N.C., Jeon, M.-J., Bettenhausen, C., Sayer, A.M., Hansell, R., Seftor, C.S.,
789 Huang, J., Tsay, S.-C., 2013. Enhanced Deep Blue aerosol retrieval algorithm: The
790 second generation: J Geophys. Res. 118, 9296–9315.

791

792 INEGI (Instituto Nacional de Estadística, Geografía y Informática), México, 2001.
793 Sistema   de   Topoformas.   Available   online   at
794 http://en.www.inegi.org.mx/temas/fisiografia/default.html#Downloads Accessed 25th
795 May 2020.

796

797 Kandakji, T., Gill, T.E., Lee, J.A., 2020. Identifying and characterizing dust point
798 sources in the southwestern United States using remote sensing and GIS.
799 Geomorphology 353, 107019.

800

801 Kaufman, Y.J., Tanré, D., Boucher, O., 2002. A satellite view of aerosols in the
802 climate system. Nature 419, 215-223.

803

804 King, J., Etyemezian, V., Sweeney, M., Buck, B.J., Nikolich, G., 2011. Dust emission
805 variability at the Salton Sea, California, USA. Aeolian Res. 3, 67-79.

806

807 Klose, M., Gill, T.E., Etyemezian, V., Nikolich, G., Zadeh, Z.G., Webb, N.P., Van
808 Pelt, R.S., 2019. Dust emission from crusted surfaces: insights from field
809 measurements and modelling. Aeolian Res. 40, 1–14.

810

811 Kocurek, G., Lancaster, N., 1999. Aeolian system sediment state: Theory and
812 Mojave Desert Kelso dune field example. Sedimentology, 46, 505–515.

813

814 Kok, J.F., Mahowald, N.M., Albani, S., Fratini, G., Gillies, J.A., Ishizuka, M., Leys,
815 J.F., Mikami, M., Park, M.S., Park, S.U., Van Pelt, R.S., 2014. An improved dust
816 emission model with insights into the global dust cycle's climate sensitivity. Atmos.
817 Chem. Phys. 14, 13023–13041.

818

819 Kondragunta, S., Zhang, H., Ciren, P., Laszlo, I., Tong, D., 2018. Tracking Dust
820 Storms Using the Latest Satellite Technology: The Rapid Refresh GOES-16
821 Advanced Baseline Imager. EM: Mag. Env. Manag. (Air Waste Manag. Assoc.), May
822 2018, 25-30.

823

824 Kopacz, J.R., Herschitz, R., Roney, J., 2020. Small satellites: an overview and
825 assessment. Acta Astronaut. 170, 93-105.

826

827 Lancaster, N., Baas, A., 1998. Influence of vegetation cover on sand transport by
828 wind: field studies at Owens Lake, California. Earth Surf. Proc. Landf. 23, 69-82.

829

830 Lee, J.A., Gill, T.E., Mulligan, K.R., Dominguez Acosta, M., Perez, A.E., 2009. Land
831 use/land cover and point sources of the 15 December 2003 dust storm in
832 southwestern North America. Geomorphology 105, 18–27.

833

834 Lee, J.A., Baddock, M.C., Mbuh, M.J., Gill, T.E., 2012. Geomorphic and land cover
835 characteristics of aeolian dust sources in west Texas and eastern New Mexico,
836 USA. Aeolian Res. 3, 459–466.

837

838 Li, J., Roy, D.P., 2017. A global analysis of Sentinel-2A, Sentinel-2B and Landsat-8
839 data revisit intervals and implications for terrestrial monitoring. Remote Sens. 9, 902.

840

841 Li, J., Kandakji, T., Lee, J.A., Tatarko, J., Blackwell III, J., Gill, T.E., Collins, J.D.,
842 2018. Blowing dust and highway safety in the southwestern United States:
843 characteristics of dust emission "hotspots" and management implications. Sci. Total
844 Environ. 621, 1023–1032.

845

846 Liu, S., Hodgson, M.E., 2016. Satellite image collection modeling for large area
847 hazard emergency response. ISPRS J. Photogramm. Remote Sens. 118, 13-21.

848

849 Mahowald, N.M., Bryant, R.G., del Corral, J., Steinberger, L., 2003. Ephemeral lakes
850 and desert dust sources. Geophys. Res. Lett. 30, 1074.

851

852 Mahowald, N.M., Kloster, S., Engelstaedter, S., Moore, J.K., Mukhopadhyay, S.,
853 McConnell, J.R., Albani, S., Doney, S.C., Bhattacharya, A., Curran, M.A.J., Flanner,
854 M.G., Hoffman, F.M., Lawrence, D.M., Lindsay, K., Mayewski, P.A., Neff, J.,
855 Rothenberg, D., Thomas, E., Thornton, P.E., Zender, C.S., 2010. Observed 20th
856 century desert dust variability: Impact on climate and biogeochemistry. Atmos.
857 Chem. Phys. 10, 10875-10893.

858

859 Miller, S.D., 2003. A consolidated technique for enhancing desert dust storms with
860 MODIS. Geophys. Res. Lett. 30, 2071.

861

862 Miller, M.E., Bowker, M.A., Reynolds, R.L., Goldstein, H.L., 2012. Post-fire land
863 treatments and wind erosion - Lessons from the Milford Flat Fire, UT, USA. Aeolian
864 Res. 7, 29-44.
865
866 Muhs, D.R., Prospero, J.M., Baddock, M.C., Gill T.E., 2014. Identifying sources of
867 aeolian mineral dust: present and past. In: Stuut, J.-B., Knippertz P. (Eds.), Mineral
868 dust – a key player in the Earth system. Springer, Berlin. pp. 51-74.
869
870 Murray, J.E., Brindley, H.E., Bryant, R.G., Russell, J.E., Jenkins, K.F., Washington,
871 R., 2016. Enhancing weak transient signals in SEVIRI false color imagery:
872 application to dust source detection in southern Africa. J. Geophys. Res. 121,
873 10199-10219.
874
875 Novlan, D.J., Hardiman, M., Gill, T.E., 2007. A synoptic climatology of blowing dust
876 events in El Paso, Texas from 1932–2005. Preprints, 16th Conf. on Applied
877 Climatology, Amer. Meteorol. Soc., J3.12.
878
879 Nicoll, K., Hahnenberger, M., Goldstein, H.L., 2020. 'Dust in the wind' from source-
880 to-sink: Analysis of the 14-15 April 2015 storm in Utah. Aeolian Res. 46, 100532.
881
882 O'Loingsigh, T., McTainsh, G.H., Tapper, N.J., Shinkfield, P., 2010. Lost in code: a
883 critical analysis of using meteorological data for wind erosion monitoring. Aeolian
884 Res. 2, 49-57.
885
886 O'Loingsigh, T., Mitchell, R.M., Campbell, S.K., Drake, N.A., McTainsh, G.H.,
887 Tapper, N.J., Dunkerley, D.L., 2015. Correction of dust event frequency from MODIS
888 Quick-Look imagery using in-situ aerosol measurements over the Lake Eyre Basin,
889 Australia. Rem. Sens. Environ. 169, 222-231.
890
891 Parajuli, S.P., Zender, C.S., 2017, Connecting geomorphology to dust emission
892 through high-resolution mapping of global land cover and sediment supply. Aeolian
893 Res. 27, 47–65.
894
895 Parajuli, S.P., Yang, Z.L., Kocurek, G., 2014, Mapping erodibility in dust source
896 regions based on geomorphology, meteorology, and remote sensing. J. Geophys.
897 Res. 119, 1977-1994.
898
899 Park, S.H., Jung, H.S., Lee, M.J., Lee, W.J., Choi, M.J., 2019. Oil Spill Detection
900 from PlanetScope Satellite Image: Application to Oil Spill Accident near Ras Al Zour
901 Area, Kuwait in August 2017. J. Coastal Res. Supp. 90, 251-260.

Planet Labs, 2020. Imagery and Archive details, available at: https://www.planet.com/products/planet-imagery/ [Accessed 1st June 2020]

Plekhov, D., Levine, E.I., 2018. Assessing the effects of severe weather events through remote sensing on Samothrace, Greece: applications for management of cultural resources. J. Arch. Sci. Rep. 21, 810-820.

Prospero, J.M., Ginoux, P., Torres, O., Nicholson, S.E., Gill, T.E., 2002. Environmental characterization of global sources of atmospheric soil dust identified with the Nimbus 7 Total Ozone Mapping Spectrometer (TOMS) absorbing aerosol product. Rev. Geophys. 40, 1002.

Reynolds, R.L., Yount, J.C., Reheis, M., Goldstein, H., Chavez, P. Jr., Fulton, R., Whitney, J., Fuller, C., Forester, R.M., 2007. Dust emission from wet and dry playas in the Mojave Desert, USA. Earth Surf. Proc. Landf. 32, 1811 – 1827.

Richter, D., Gill, T., 2018. Challenges and opportunities in atmospheric dust emission, chemistry, and transport. Bull. Am. Meteorol. Soc. 99, ES115–ES118.

Rivas, J.A. Jr., Schröder, T., Gill, T.E., Wallace, R.L., Walsh, E.J., 2019. Anemochory of diapausing stages of microinvertebrates in North American drylands. Freshwater Biol. 64, 1303-1314.

Rivera Rivera, N.I., Gill, T.E., Gebhart, K.A., Hand, J.L., Bleiweiss, M.P., Fitzgerald, R.M., 2009. Wind modeling of Chihuahuan Desert dust events. Atmos. Environ. 43, 347-354.

Rivera Rivera, N.I., Gill, T.E., Bleiweiss, M.P., Hand, J.L., 2010. Source characteristics of hazardous Chihuahuan Desert dust outbreaks. Atmos. Environ. 44, 2457–2468.

Rosen, M.R. 1994. The importance of groundwater in playas: a review of playa classifications and the sedimentology and hydrology of playas. Geol. Soc. Amer. Spec. Pap. 289, 1–18.

Schepanksi, K., Tegen, I., Laurent, B., Heinold, B., Macke A., 2007. A new Saharan dust source activation frequency map derived from MSG-SEVIRI IR-channels. Geophys. Res. Lett., 34, L18803.

942 Schepanski, K., Tegen, I., Todd, M. C., Heinold, B., Bönisch, G., Laurent, B.,
943 Macke, A., 2009. Meteorological processes forcing Saharan dust emission inferred
944 from MSG-SEVIRI observations of subdaily dust source activation and numerical
945 models. J. Geophys. Res. 114, D10201.

946

947 Schepanski, K., Tegen, I., Macke, A., 2012. Comparison of satellite based
948 observations of Saharan dust source areas. Remote Sens. Environ. 123, 90–97.

949

950 Schmetz, J., Pili, P., Tjemkes, S., Just, D., Kerkmann, J., Rota, S., Ratier, A., 2002.
951 An introduction to Meteosat second generation (MSG). Bull. Am. Meteorol. Soc. 83,
952 977-992.

953

954 Shao, Y., Wyrwoll, K.H., Chappell, A., Huang, J., Lin, Z., McTainsh, G.H., Mikami,
955 M., Tanaka, T.Y., Wang, X., Yoon, S., 2011. Dust cycle: An emerging core theme in
956 Earth system science. Aeolian Res. 2, 181–204.

957

958 Sinclair, S.N., LeGrand, S.L., 2019. Reproducibility assessment and uncertainty
959 quantification in subjective dust source mapping. Aeolian Res. 40, 42-52.

960

961 She, L., Xue, Y., Yang, X., Guang, J., Li, Y., Che, Y., Fan, C., Xie, Y., 2018, Dust
962 detection and intensity estimation using Himawari-8/AHI observation. Remote Sens.,
963 10, 490.

964

965 Sowden, M., Mueller, U., Blake, D., 2018, Review of surface particulate monitoring of
966 dust events using geostationary satellite remote sensing. Atmos. Environ. 183, 154-
967 164.

968

969 Sweeney, M.R., McDonald, E.V., Etyemezian, V., 2011, Quantifying dust emissions
970 from desert landforms, eastern Mojave Desert, USA. Geomorphology 135, 21–34.

971

972 Thomas, D.S.G., Wiggs, G.F.S., 2008. Aeolian system responses to global change:
973 challenges of scale, process and temporal integration. Earth Surf. Proc. Landf. 33,
974 1396-1418.

975

976 Thompson, D., Braverman, A., Brodrick, P.G., Candela, A., Carmon, N., Clark, R.N.,
977 Connely, D., Green, R.O., Kokaly, R.F., Li, L., Mahowald, N., Miller, R.L., Oking,
978 G.S., Painter, T.H., Swayze, G.A., Turmon, M., Susilouto, J., Wettergreen, D.S.,
979 2020. Quantifying uncertainty for remote spectroscopy of surface composition.
980 Remote Sens. Environ. 247, 111898.

981

982 Urban, F.E., Goldstein, H.L., Fulton, R., Reynolds, R.L. (2018) Unseen dust
983 emission and global dust abundance: documenting dust emission from the Mojave
984 Desert (USA) by daily remote camera imagery and wind-erosion measurements. J.
985 Geophys. Res. 123, 8735-8753.

986

987 Vickery, K.J., Eckardt, F.D., Bryant, R.G., 2013. A sub-basin scale dust plume
988 source frequency inventory for southern Africa, 2005-2008. Geophys. Res. Lett. 40,
989 5274-5279.

990

991 von Holdt, J.R., Eckardt, F.D., Wiggs, G.F.S., 2017. Landsat identifies aeolian dust
992 emission dynamics at the landform scale. Remote Sens. Environ. 198, 229–243.

993

994 von Holdt, J.R.C., Eckardt, F.D., Baddock, M.C., Wiggs, G.F.S., 2019. Assessing
995 landscape dust emission potential using combined ground- based measurements
996 and remote sensing data. J. Geophys. Res. 124, 1080-1098.

997

998 Villela, T., Costa, C.A., Brandão, A.M., Bueno, F.T., Leonardi, R., 2019. Towards the
999 thousandth CubeSat: A statistical overview. Int. J. Aerospace Eng. 2019, 063145.

1000

1001 Walker, A.L., Liu, M., Miller, S.D., Richardson, K.A., Westphal, D.L., 2009.
1002 Development of a dust source database for mesoscale forecasting in Southwest
1003 Asia. J. Geophys. Res. 114, D18207.

1004

1005 Washington, R., Todd, M., Middleton, N.J., Goudie, A.S., 2003. Dust storm source
1006 areas determined by the Total Ozone Monitoring Spectrometer and surface
1007 observations. Ann. Assoc. Am. Geog. 93, 297–313.

1008

1009 Webb, N.P., Strong, C.L., 2011. Soil erodibility dynamics and its representation for
1010 wind erosion and dust emission models. Aeolian Res. 3, 165-179.

1011

1012 Webb, N.P., Herrick, J.E., Van Zee, J.W., Courtright, E.M., Hugenholtz, C.H.,
1013 Zobeck, T.M., Okin, G.S., Clingan, S.D., Cooper, B.F., Billings, B.J, Boyd, R.,
1014 Duniway, M.C., Derner, J.D., Fox, F.A., Havstad, K.M., Heilman, P., Ludwig, N.A.,
1015 Metz, L.J., Nearing, M.A., Norfleet, M.L., Pierson, F.B., Sanderson, M.A., Sharratt,
1016 B.S., Steiner, J.L., Tatarko, J., Tedela, N.H., Toledo, D., Unnasch, R.S., Van Pelt,
1017 R.S., Wagner, L., 2016. The National Wind Erosion Research Network: building a
1018 standardized long-term data resource for aeolian research, modeling and land
1019 management. Aeolian Res. 22, 23-36.

1020

1021 Webb, N.P., Chappell, A., Edwards, B.L., McCord, S.E., Van Zee, J.W., Cooper,
1022 B.F., Courtright, E.M., Duniway, M.C., Sharratt, B., Tedela, N., Toledo, D., 2019.
1023 Reducing sampling uncertainty in aeolian research to improve change detection. J.
1024 Geophys. Res. 124, 1366-1377.

1025

1026 Wicaksono, P., Lazuardi, W., 2018. Assessment of PlanetScope images for benthic
1027 habitat and seagrass species mapping in a complex optically shallow water
1028 environment. Intl. J. Remote Sens. 39, 5739-5765.

1029

1030 Yue, H., He, C., Zhao, Y., Ma, Q., Zhang, Q., 2017. The brightness temperature
1031 adjusted dust index: An improved approach to detect dust storms using MODIS
1032 imagery. Int. J. Appl. Earth Obs. Geoinf. 57, 166-176.

1033

1034 Zender, C.S., Newman, D.J., Torres, O., 2003. Spatial heterogeneity in aeolian
1035 erodibility: Uniform, topographic, geomorphic and hydrologic hypotheses. J.
1036 Geophys. Res. 108, 4543.

1037

1038 Zhang, B., Tsunekawa, A., Tsubo, M., 2008. Contributions of sandy lands and stony
1039 deserts to long-distance dust emission in China and Mongolia during 2000-2006.
1040 Global Planet. Change 60, 487-504.

1041 FIGURE CAPTIONS

1042

1043 Figure 1: Assessments of dust source activity in the northern Chihuahuan Desert,

1044 based on different moderate resolution MODIS data. a) Contours showing long term

1045 (2003-2014) dust loading as represented by Frequency of Occurrence (FoO % days)

1046 for MODIS Dust Optical Depth >0.75 (after Baddock et al., 2016), superimposed on

1047 the preferential dust source (PDS) geomorphological classification of emission

1048 potential (Bullard et al., 2011). Dashed box indicates focus of panels (b) and (c). b)

1049 Inventory of dust plume origin points 2001-2009 for the study region, as derived from

1050 inspection of true-colour MODIS scenes (Baddock et al., 2011), superimposed on

1051 the same PDS geomorphological classification (1b – ephemeral lake, 1d – dry, non-

1052 consolidated lake, 2d – high relief (unarmoured, unincised) alluvial systems, 3d –

1053 low relief (unarmoured, unincised) alluvial systems, 5b – aeolian sand dunes, 7 low

1054 emission surfaces) c) Example true-colour MODIS dust scene of a regional emission

1055 event (27th November 2005) with plume origins marked. The extent of the Bolson de

1056 los Muertos playa is shown, with the blue crosshatch indicating the Rio Santa Maria

1057 paleo-delta feeding into the playa. Dashed box indicates focus of Figure 2(c,d) in the

1058 southwestern arm of the playa.

1059

1060

1061

1062

1063

1064

1065

1066

1067

1068

1069 Figure 2 a) Terra MODIS (1735 UTC) true-colour scene of 30th November 2018 dust

1070 event showing the faint presence of dust visible on the south-western lobe of the of

1071 Bolson de los Muertos playa. Red box highlights the plume over the playa surface,

1072 before presence of cloud to the east obscures plume. Plume interpreted with a

1073 comparison to dust-free MODIS scene (not shown). Hashed lines show extent of the

1074 Rio Santa Maria paleo-delta from INEGI (2001) national soil map. Pixel resolution

1075 250 m. Dashed black box shows focus of figure panels (c) and (d). b) Aqua MODIS

1076 (2050 UTC) from the same day showing presence of a more apparent dust plume

1077 slightly further to the north in the focus area. Red box highlights plume extending to

1078 the east. Dashed yellow box shows focus of Figure 5. c) PlanetScope (1706 UTC)

1079 true colour scene of 30th November 2018 dust event, showing emission occurring in

1080 the south-western arm of Bolson de los Muertos playa. Pixel resolution 3 m. Note

1081 some cloud is present, but less than shown in MODIS at 1735 UTC. (A high

1082 resolution version of this panel is available in the Supplementary Material.) d) Grid

1083 cells where surface emission can be estimated from plumes identifiable in

1084 PlanetScope, for a regular 100 x 100 m grid over the southwest arm of the Bolson

1085 de los Muertos. Solid cells – cells containing discernible upwind initiation points of

1086 small plumes shown in (c). Open cells – cells with evidence of likely emission from

1087 the surface, shown by multiple individual small scale plumes, close to the surface,

1088 and located downwind of solid cells containing discernible initiation. Black triangle

1089 and circle indicate apparent plume source estimated from Terra and Aqua images

1090 (a, b) respectively.

1091

1092

1093

1094

1095

1096

1097

1098   Figure 3: True colour PlanetScope scene (27th November 2018, 1722 UTC)

1099   depicting focus section of the southwest arm of the Bolson de los Muertos playa

1100   surface three days before the dust event in Figure 2. Solid squares are the upwind

1101   emitting grid cells, open green polygons are the broader downwind estimates of

1102   emitting surface from Figure 2d.

1103

1104

1105

1106

1107

1108

1109

1110

1111

1112

1113

1114

1115

1116

1117

1118

1119

1120

1121

1122 Figure 4: Conceptual figure characterising time and spatial scales of dust emission
1123 and dust transport (i.e. plume passage) phenomena, in relation to the
1124 monitoring/detection capabilities of existing satellite systems, and the niche of
1125 CubeSats (e.g. PlanetScope), from this study. We use the spatial scale limits
1126 suggested by Strong and Webb (2011) to highlight that the spatial resolution, in
1127 which most remote sensing observations operate, obviates plot-scale of
1128 understanding dust emission processes. In the temporal, most studies are unable to
1129 sample at a scale where a representative sample of dust events will be captured,
1130 compared to field-based (e.g. Klose et al., 2019) or meteorological data-based (e.g.
1131 O'Loingsigh et al., 2010) approaches. Black boxes represent realistic limits in dust
1132 source/plume detection based upon published studies (A: TOMS, Bryant et al.,
1133 2007; B: SEVIRI, Murray et al. 2016; C: MODIS, Baddock et al., 2009; D:
1134 Landsat/Sentinel, von Holdt et al., 2017; Bakker et al., 2019, E:
1135 CubeSat/PlanetScope; this study.)

1136

1137

1138

1139

1140

1141

1142

1143

1144

1145

1146

1147

1148

1149 Figure 5: PlanetScope overpasses available 11 minutes apart, achieved by the
1150 Planet CubeSat constellation for the 30th November 2018 regional dust event. The
1151 image sequence helps constrain the spatial occurrence and temporal onset of dust
1152 emission from centre-pivot irrigated field systems during the day's dust event. A
1153 1003 MST (1703 UTC) overpass was also available for this site. Area of focus is
1154 shown by yellow box in Figure 2b.

Graphical Abstract

- Remote sensing has enabled key characterisations of mineral dust sources globally

- Moderate-resolution sensors cannot be reconciled with field study of dust emission

- New CubeSat technology allows observation of active emission processes

- Potential for sub-daily source monitoring from sensors in constellations

- We call for the systematic application of CubeSat imagery over dust sources
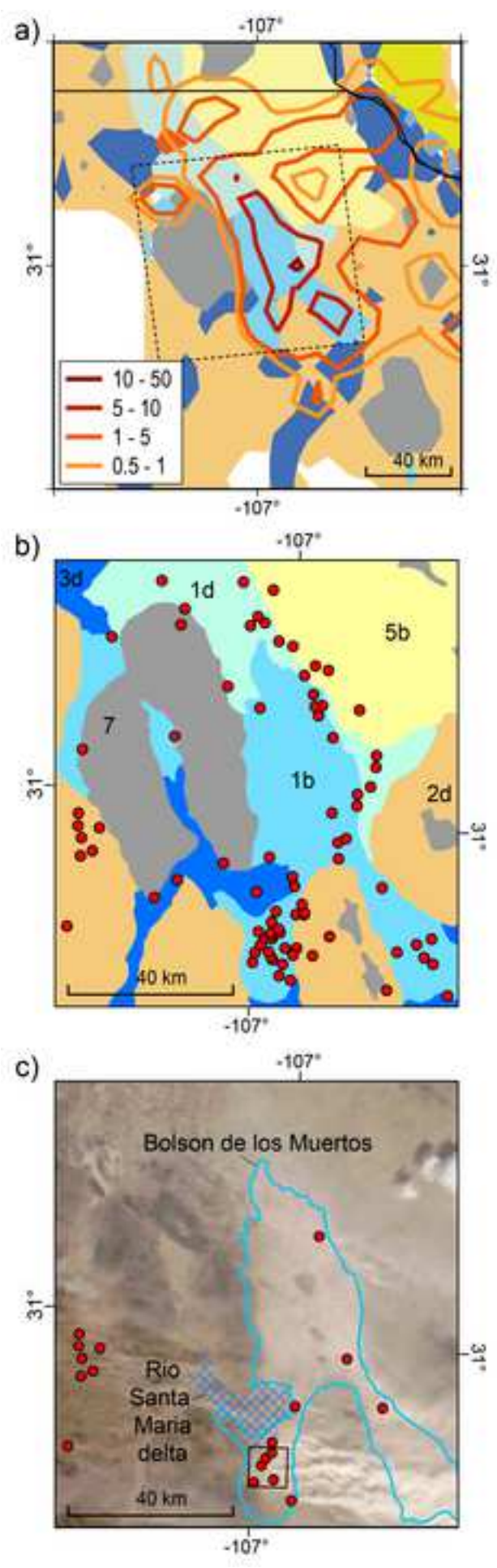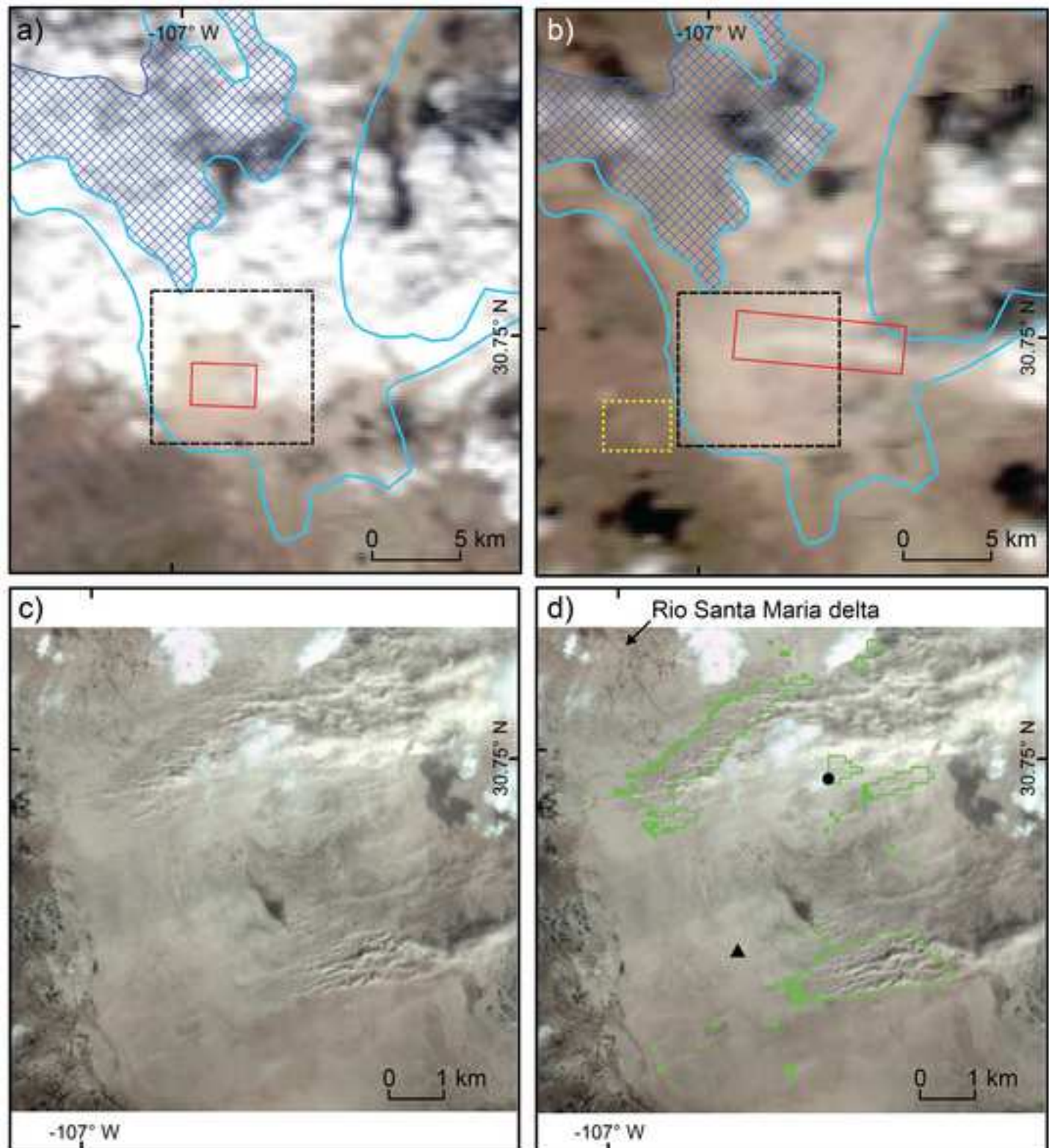
Figure 3
Click here to download high resolution image
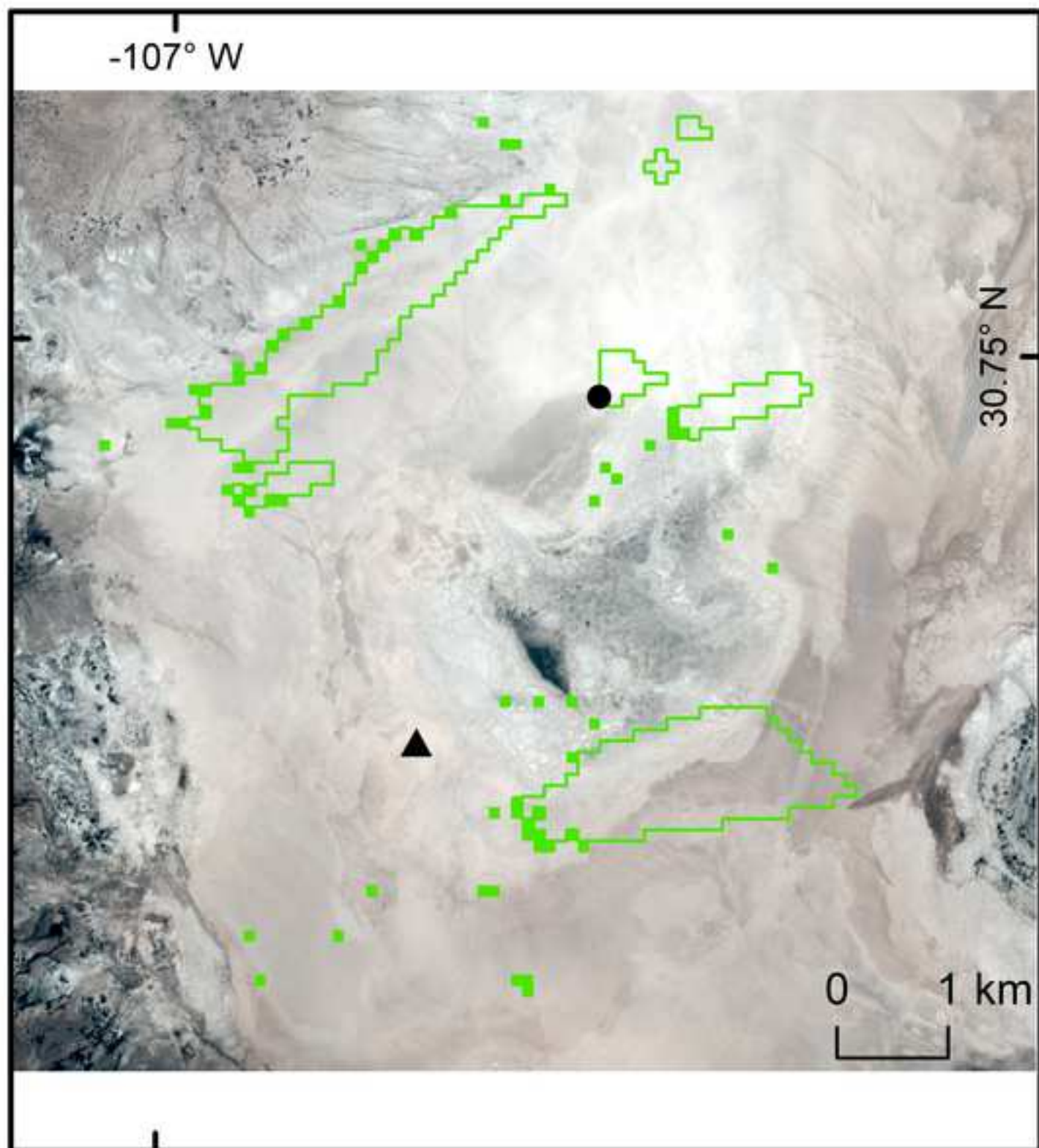
Figure 4
Click here to download high resolution image

Figure 5
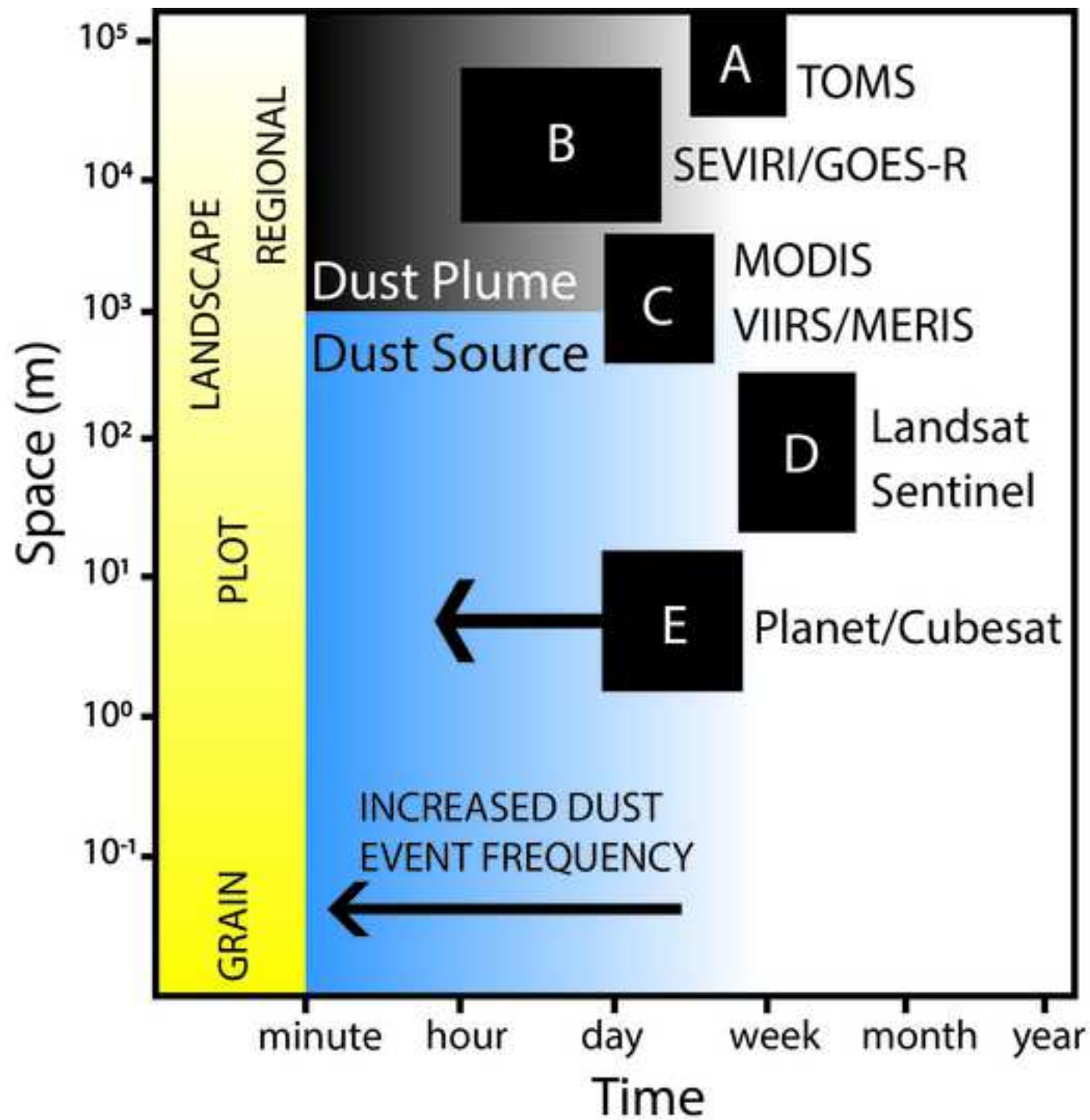[Click here to download high resolution image](#)
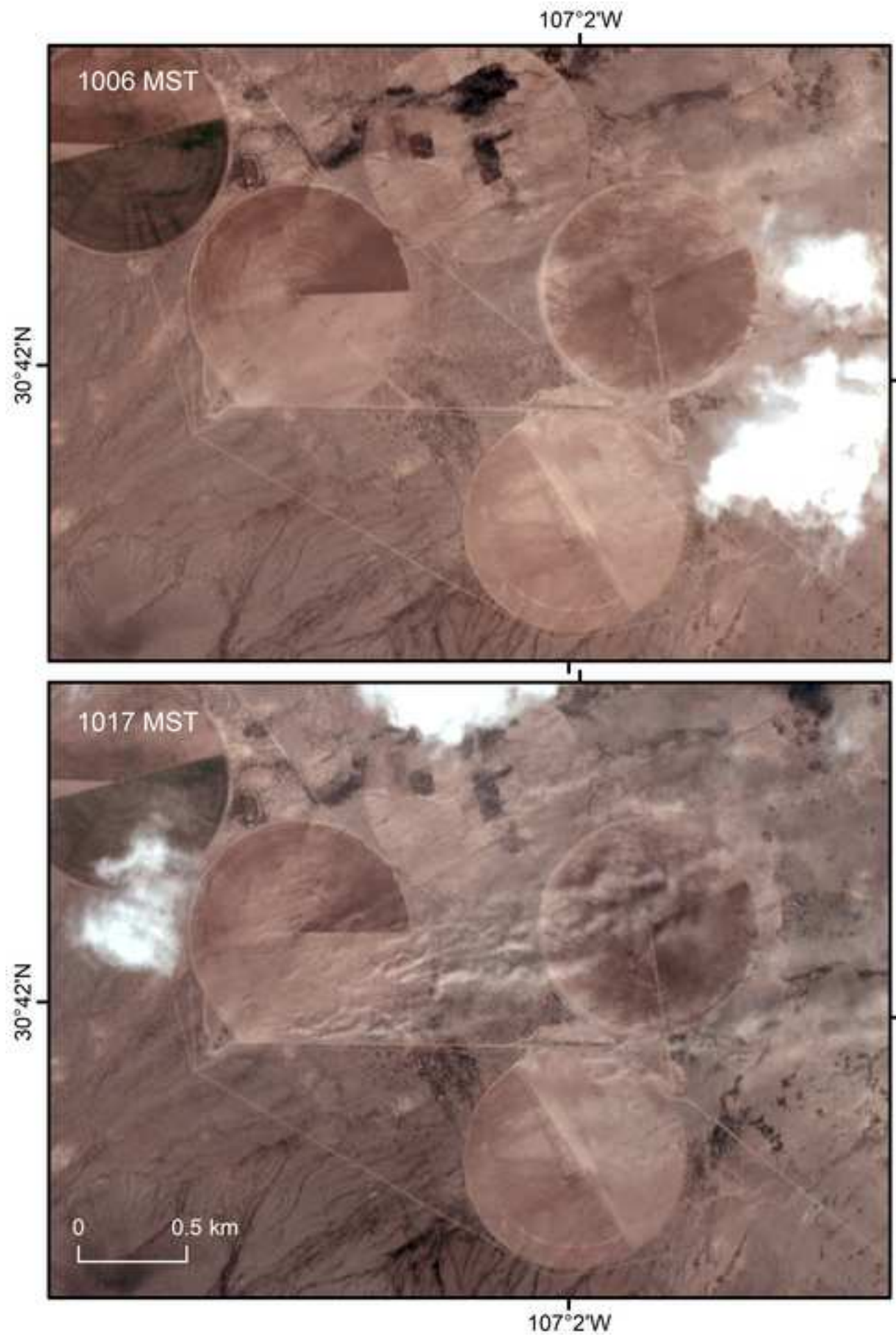
Figure 5

*Credit Author Statement

Matthew Baddock: Conceptalization, Methodology, Formal Analysis, Writing – Original Draft. **Robert Bryant:** Conceptalization, Methodology, Writing – Original Draft. **Miguel Dominguez Acosta**: Writing – Original Draft, Writing – Review & Editing. **Thomas Gill**: Conceptalization, Methodology, Writing – Original Draft.

Declaration of interests

☒ The authors declare that they have no known competing financial interests or personal relationships that could have appeared to influence the work reported in this paper.

☐The authors declare the following financial interests/personal relationships which may be considered as potential competing interests: